Research Square

Preprints are preliminary reports that have not undergone peer review.
They should not be considered conclusive, used to inform clinical practice,
or referenced by the media as validated information.

Mechanistic study on PSMB9 and HLA-F regulating polyamine metabolism to mediate the malignant progression of glioma

Yan Cheng

chengyan211@163.com

Shanxi Provincial People's Hospital

Lin Zhang

Shanxi Provincial People's Hospital

Lina Zheng

Shanxi Provincial People's Hospital

Ting Wang

Shanxi Provincial People's Hospital

Weiwei Zhang

Shanxi Provincial People's Hospital

Research Article

Keywords: Glioma, Glioblastoma multiforme and lower grade glioma, Polyamine metabolism, PSMB9, HLA-F

Posted Date: September 15th, 2026

DOI: https://doi.org/10.21203/rs.3.rs-11007848/v1

License: This work is licensed under a Creative Commons Attribution 4.0 International License.
Read Full License

Additional Declarations: No competing interests reported.

Mechanistic study on PSMB9 and HLA-F regulating polyamine metabolism to mediate the malignant progression of glioma

Yan Cheng[1]*, Lin Zhang[1], Lina Zheng[1], Ting Wang[1], Weiwei Zhang[1]

[1]Department of Anesthesiology, Shanxi Provincial People's Hospital, Taiyuan, Shanxi, China

* Correspondence:

Yan Cheng

chengyan211@163.com

Running title: PSMB9-HLA-F Axis in Glioma Progression

Abstract

Polyamine metabolism correlates with tumor progression, yet its regulatory networks in glioblastoma multiforme and lower grade glioma (GBMLGG) remain unclear. This study aimed to screen polyamine metabolism related gene (PMRG)-related prognostic biomarkers in glioma malignant progression. First, GBMLGG-ralated datasets were acquired from the Cancer Genome Atlas (TCGA) and the Chinese Glioma Genome Atlas (CGGA). Ten core prognostic PMRGs were screened via differential expression and univariate Cox regression, with PSMB9 highly expressed and correlated with adverse clinical features and poor prognosis in both cohorts. PSMB9 overexpression promoted glioma cell malignant phenotypes *in vitro* while knockdown inhibited them, as verified by Reverse Transcription Quantitative Polymerase Chain Reaction (RT-qPCR) and Western Blot (WB) in cell lines, and its high expression was associated with abnormal immune infiltration, immune escape, distinct mutation profiles and increased camptothecin sensitivity. Subsequently, HLA-F was confirmed as PSMB9's key downstream gene via Protein-Protein Interaction (PPI) network and Spearman correlation from transcriptome

sequencing of knockdown cells, with regulatory relationships verified by functional experiments, and PSMB9 drove glioma malignancy by regulating HLA-F. Finally, *in vivo* nude mouse assays confirmed PSMB9 knockdown reduced tumor growth, and joint survival analysis showed co-high expression of PSMB9 and downstream genes enhanced poor prognosis prediction. In conclusion, PSMB9 is a novel prognostic biomarker and oncogene in GBMLGG that drives malignancy via HLA-F regulation. The PSMB9-HLA-F axis represents a potential therapeutic target, and their co-expression enhances prognostic prediction.

Keywords: Glioma, Glioblastoma multiforme and lower grade glioma, Polyamine metabolism, PSMB9, HLA-F

1 Introduction

Glioma, the most common primary brain tumor, accounts for ~30% of all and 80% of malignant primary brain tumors, and is the leading cause of death in these patients [1]. The standardized treatment for glioma mainly includes maximal safe surgical resection, postoperative adjuvant radiotherapy and chemotherapy [2]. Although surgical methods and chemotherapy drugs have been studied and improved over the years [3], the long-term prognosis of glioma patients has been no significant improved due to the invasive growth, strong aggressiveness, and high recurrence rate of glioma [4,5]. The median overall survival (mOS) of the patients usually less than two years and 5-year survival rate less than 5% [6]. Therefore, it is of great significance to improve the clinical outcome of patients by exploring the key molecular mechanisms of glioma development and screening new prognostic markers and therapeutic targets.

Polyamines are small cationic alkylamines that are ubiquitous in eukaryotic and prokaryotic cell

metabolism. They are essential auxins in the process of cell proliferation [7]. Excessive intracellular polyamine can lead to excessive cell proliferation. Researchs indicate that the occurrence and development of tumors are closely related to abnormal polyamine metabolism [8,9]. In normal cells, polyamine homeostasis is strictly controlled under the feedback regulation of the polyamine metabolic network. However, in tumor cells, this homeostasis is often disrupted [10]. The growth and progression of tumors both require high levels of polyamines, which promote the proliferation, invasion, and metastasis of tumor cells [11]. The effect of the expression level of polyamine metabolic pathway-related genes on tumors has been confirmed in a variety of tumors. In breast cancer, polyamines play a crucial role in regulating cell growth, differentiation, apoptosis, and DNA/protein synthesis [12]. In neuroblastoma, elevated expression of polyamine synthesis genes leads to increased polyamine production and lower survival rates [13]. The influence of polyamine metabolism in glioma has also been reported. Research indicates that the activity of ornithine decarboxylase (ODC), the first key enzyme in polyamine metabolism, serves as a biochemical biomarker representing the malignant degree of brain tumors [14]. Given the lack of research on polyamine metabolism-related signaling pathways in glioma cells, the identification of accurate therapeutic targets remains challenging. To address this gap, the present study aims to screen polyamine metabolism-related prognostic biomarkers and explore their molecular mechanisms in glioma malignant progression.

This study aims to screen polyamine metabolism-related core biomarkers via bioinformatics, verify their expression and prognostic value in glioma, clarify their impact on malignant phenotypes, explore the regulatory relationship between biomarkers and key downstream genes as well as their mechanisms in polyamine metabolism, and ultimately elucidate the molecular mechanism by which polyamine metabolism drives glioma malignant progression, providing new theoretical basis and potential targets

for prognostic evaluation and targeted therapy.

2 Materials and methods

2.1 Data sources

The training set was constructed from UCSC Xena (https://xenabrowser.net/datapages/) by downloading transcriptome, clinical and follow-up data [age, gender, Isocitrate Dehydrogenase (IDH) mutation, O6-Methylguanine-DNA Methyltransferase (MGMT) methylation, tumor grade, survival time] for The Cancer Genome Atlas Glioblastoma Multiforme (TCGA-GBM) and The Cancer Genome Atlas Lower Grade Glioma (TCGA-LGG), which were merged into TCGA-GBMLGG (702 samples). Only 01A (tumor) and 11A (normal/paracancerous) samples were retained, yielding 649 samples (644 GBMLGG vs 5 control), with 638 GBMLGG cases having survival data. The validation set from the Chinese Glioma Genome Atlas (CGGA, http://www.cgga.org.cn/) comprised 693 samples, with 657 tumor cases matched with survival information. For polyamine metabolism-related genes (PMRGs), the term "polyamines" was searched in MSigDB (https://www.gsea-msigdb.org/gsea/msigdb), retrieving the REACTOME: Polyamine Metabolism gene set of 59 PMRGs.

2.2 Differential expression analysis

First, Wilcoxon test compared PMRG transcript levels between GBMLGG and normal controls. PMRGs with extremely low expression were filtered out. R package ggplot2 (v3.3.6) [15] generated box plots, and differentially expressed PMRGs (DE-PMRGs) were selected. Next, univariate Cox regression was applied to DE-PMRGs in training set GBMLGG samples using R package survival (v3.4-0) [16]. Variables with hazard ratio (HR) $\neq 1$ and $P < 0.05$ were selected. Genes showing inconsistent directions between survival HR and differential fold change (FC) were excluded, and the remaining ones were defined as candidate genes. Finally, surv_cutpoint via R package survminer

(v0.4.9) [17] determined the optimal threshold. Median expression of candidate genes served as the cutoff to classify samples into high- and low-expression subsets in training (TCGA-GBMLGG) and validation (CGGA) sets. Survival distributions were evaluated by log-rank test with HR calculation, and genes with consistent HR directions and significant differences in both cohorts were selected as candidate biomarkers.

2.3 *In vitro* experiment

2.3.1 Cell culture

SVG P12 human astrocytes (SNL-650) were purchased from Shanen Biotechnology; U87 human glioblastoma cells (IM-H211), T98G (IM-H211) and U251 (IM-H328) human glioma cells were from Yimo Biotechnology. All cells were of human brain origin: SVG P12 was fibroblast-like, while the other three were epithelial-like, all adherent. Standard culture used DMEM-based medium with 10% FBS and 1% penicillin-streptomycin; U87, T98G and U251 were maintained in 90% DMEM. All cells were incubated at 37°C with 5% CO_2, subcultured at 1:2-1:3 ratios two to three times weekly, and cryopreserved in serum-free medium in liquid nitrogen.

2.3.2 Reverse Transcription Quantitative Polymerase Chain Reaction (RT-qPCR)

Total RNA was isolated using FastPure Complex Tissue/Cell Total RNA Isolation Kit (Vazyme, RC113-01) following the provided instructions, and the concentration was quantified using a Nanodrop-500 (Allsheng, Nano500). RNA was then reverse transcribed into cDNA with ABScript III RT Master Mix for RT-qPCR with gDNA Remover (Abclonal, RK20429) for RT-qPCR assay, which was employed via Genious 2X SYBR Green Fast RT-qPCR Mix (Abclonal, RK21205). The expression level of genes was normalized into GAPDH, and calculated using $2^{-\Delta\Delta Ct}$ method. The primer sequences used in this analysis were all listed in **Table S1**.

2.3.3 Cell modeling and verification

Glioma cell models with biomarker knockdown/overexpression were established (primer sequences in **Table S2**). 293T cells were transfected with target gene DNA, pMD2.G (0.25 μg) and psPAX2 (0.75 μg) using jetPRIME® transfection reagent (Polyplus, 101000025). Viral supernatant was collected, filtered (0.22 μm) and stored at -80°C. T98G cells were infected with virus plus 5 μg/mL polybrene, and stable lines were selected by antibiotics. RT-qPCR verified biomarker mRNA levels in knockdown and overexpression groups. For Western blot (WB), cells were lysed in RIPA buffer with 1% PMSF, protein quantified by BCA assay, followed by SDS-PAGE, membrane transfer, antibody incubation, ECL exposure and quantitative analysis (ImageJ) per standard protocols.

2.3.4 The influence of biomarker on cell biological behaviors

After verifying PSMB9 knockdown/overexpression, cell viability was assessed by CCK-8 assay per manufacturer's protocol; migration, invasion and colony formation were evaluated by Scratch assay (6×10^4 cells/well, serum-free, photographed under 4× microscope, scratch width analyzed by ImageJ), Transwell assay with Corning® Matrigel® matrix (Corning, 356234), and colony formation with crystal violet staining, respectively. All quantitative analyses used ImageJ.

2.4 Expression and survival analysis

To evaluate biomarker expression and prognostic significance, Wilcoxon test compared expression between disease and control groups in the training set. Survival differences between expression subgroups in training and CGGA validation sets were assessed via R packages survival and survminer, with Kaplan-Meier (KM) curves generated. In disease samples from both cohorts, expression was ranked, optimal cut-off determined by surv_cutpoint, and survival curves compared by log-rank test.

2.5 Clinical and molecular mechanism analysis

To explore biomarker expression correlations with clinical features and transcriptome, violin plots across subgroups were generated using the R package ggplot2. Clinical characteristic proportions were compared between high- and low-expression cohorts and displayed graphically. Spearman correlation analysis calculated biomarker-transcriptome gene correlations. Gene Set Enrichment Analysis (GSEA) was performed using R package clusterProfiler (v4.7.1.001) [18] based on MSigDB KEGG gene set (c2.cp.kegg.v2023.2.Hs.symbols.gmt), with significant sets filtered by |NES| >1 and P <0.05. Gene Set Variation Analysis via the R package GSVA (v1.44.5) [19] enrichment scores were derived for high- vs low-expression samples via R package GSVA, followed by differential analysis (|t| >2, P <0.05) using R package limma (v3.52.4) [20]. R package limma identified DEGs between biomarker high- and low-expression groups [$|\log_2 FC| >1$, adj.P <0.05], with volcano plots generated by R package ggplot2. DEGs underwent functional annotation via overrepresentation analysis of Gene Ontology (GO) biological processes and Kyoto Encyclopedia of Genes and Genomes (KEGG) pathways using clusterProfiler (adj.P <0.05). R package enrichplot were used to visualize the top 8 GO terms in biological process (BP), cellular component (CC) and molecular function (MF), and top 15 KEGG pathways.

2.6 Immune-related analysis

To explore biomarker's immunological role, immune cell proportions in high/low expression samples were calculated via R package CIBERSORT (v1.03) [21], with stacked bar charts and box plots generated by R package ggh4x (v0.3.1) [15] and intergroup comparisons by Wilcoxon test. Tumor Immune Dysfunction and Exclusion (TIDE) scores were obtained from the TIDE platform (http://tide.dfci.harvard.edu/), with group differences assessed by Wilcoxon test and Spearman correlation between biomarker expression and TIDE scores analyzed by scatter plots. ImmuneScore,

StromalScore and Estimate score[22] were calculated via R package estimate (v1.0.13) [23], with Wilcoxon tests for score differences and violin plots. Meanwhile, the R package ImmuneSubtypeClassifier (v0.1.0) [24] was utilized to assign disease samples to six predefined immune phenotypes: C1 (wound healing), C2 (IFN-γ dominant), C3 (inflammatory), C4 (lymphocyte-depleted), C5 (immune-quiescent), and C6 (TGF-β dominant), and biomarker expression across subtypes was compared using Wilcoxon tests with violin plots.

2.7 Mutation and drug sensitivity analysis

With a view to characterizing biomarker-related genetic mutations and drug sensitivity, training set disease sample mutations are analyzed via R package maftools (v2.12.0) [25], with waterfall plots illustrating mutational profiles of the 20 most prevalent genes were generated for expression-based subgroups.

Half-maximal inhibitory concentrations (IC_{50}) were calculated for 198 cancer therapeutic compounds using pharmacogenomic data from the Genomics of Drug Sensitivity in Cancer (GDSC) database (https://www.cancerrxgene.org/) using R package oncoPredict (v0.2) [26], and these inhibitory concentration metrics were compared across biomarker-stratified subgroups (high vs. low expression) via Wilcoxon rank-sum analysis.

2.8 Transcriptome data processing and differential analysis

For the sake of profiling gene expression differences between tumor stable and parental cells, total RNA was purified from specimens using TRIzol (Thermo Fisher, 15596018) following the supplier's recommended procedure. RNA quantity and purity are assessed by NanoDrop ND-1000, while RNA integrity is checked with Bioanalyzer 2100. mRNA is captured by Dynabeads Oligo (dT) (cat.25-61005), fragmented by magnesium ion fragmentation kit at 94℃ for 5-7 minutes, and reverse

transcribed to cDNA. Second-strand synthesis is completed with E. coli DNA polymerase I and RNase H with 2'-deoxyuridine-5'-triphosphate (dUTP) Solution incorporated, followed by end repair, A-tailing, T-adapter ligation and magnetic bead purification. Next, after Uracil-DNA Glycosylase (UDG) enzyme digestion of the second strand, PCR amplification is performed under the conditions: 95℃ for 3 min, 8 cycles of 98℃ (15 s), 60℃ (15 s), 72℃ (30 s), final extension 72℃ for 5 min. Strand-specific libraries with insert size 300bp ± 50bp are built and sequenced on Illumina NovaSeq^{TM} 6000 PE150. Raw fastq files are filtered by FastQC to generate clean data, which is aligned to Homo_sapiens.GRCh38, quantified with featureCounts, and converted to TPM values using the TPM formula [27]. Differential gene expression between T98G-SH-biomarker and T98G is analyzed via the DESeq2 package in R, with genes filtered by $|\log_2 FC| > 1$ and $adj.P < 0.05$. Finally, volcano plot visualization was performed with ggplot2, whereas heatmap generation employed ComplexHeatmap.

2.9 Protein-Protein Interaction (PPI) and correlation screening

With the intent of unraveling connections between biomarker and its associated DEGs, a PPI network is constructed for biomarker-DEGs and biomarker via the STRING database (http://string.embl.de/). A confidence score of 0.4 is applied to filter proteins interacting with biomarker, and Spearman correlation analysis between biomarker and these filtered interacting proteins is conducted using R package psych based on self-sequenced transcriptome data. Pairs were filtered based on stringent criteria: absolute correlation > 0.9 and statistical significance ($P < 0.05$).

2.10 Validation and screening of the key gene for expression quantity

For the objective of validating expression patterns and identifying key gene tied to biomarker, expression levels of genes interacting with and strongly correlated to biomarker are assessed in both the self-sequenced transcriptome dataset and the training TCGA-GBMLGG dataset. Genes with no

expression in either dataset are excluded, and those displaying opposite expression trends with significant differences across both datasets are designated as key gene, with KM curves generated for this key gene.

2.11 *In vitro* experiment

2.11.1 Screening of key gene by RT-qPCR

The specific experimental procedures are consistent with those described in Section 2.3.2. The primer sequences are shown in **Table S3**.

2.11.2 Cell modelling and the influence of key gene on cell biological behaviors

Key gene knockdown and overexpression cell models were constructed (primer sequences in **Table S4**), and the regulatory effect of key gene on biological behaviors of biomarker-knockdown T98G cells was investigated. Experimental procedures were consistent with those described in Sections 2.3.3 and 2.3.4.

2.12 *In vivo* tumorigenesis experiment

Logarithmically growing cells were collected, washed with PBS (3×), and resuspended in serum-free medium to 10^7 cells/mL at 4°C. Twelve male Balb/c nude mice [5-6 weeks old, Specific Pathogen-Free (SPF)] from Hangzhou Qizhen Laboratory Animal Science and Technology Co., Ltd. [SCXK(Zhejiang)2022-0005, 20251031Abzz010099900009] were used. All animal experiments were approved by the Animal Ethics Committee of Dr.Can Biotechnology (Zhejiang) Co., Ltd., Approval No. DRK-20251020212. For xenograft establishment, cell-Matrigel mixture (1:1 in 200 μL PBS) was injected subcutaneously into the right forelimb axilla. Tumor dimensions were measured every 5 days with calipers, and volume calculated as $V = 0.5 \times L \times W^2$. After experiments, mice were euthanized by cervical dislocation per institutional guidelines; tumors were dissected, rinsed with saline, dried, weighed, sized, and photographed. Specimens were flash-frozen in liquid nitrogen and stored at -80°C.

2.13 Joint analysis of biomarker and key gene

Samples in the training TCGA-GBMLGG dataset were divided into four groups based on biomarker and key gene expression levels: high_high, high_low, low_high, and low_low. KM curves were plotted to compare survival across the four groups.

2.14 Statistic analysis

Statistical analyses used SPSS (v19.0) for conventional statistics and R (v4.2.2) for bioinformatics. Normally distributed data were mean±SD (t-test); non-normal data were median (P25-P75) (Mann-Whitney U). Multi-group comparisons used Kruskal-Wallis; categorical data used chi-square test. Graphs were plotted with GraphPad Prism (v9.0). $P<0.05$ was significant.

3 Results

3.1 Screening of 10 polyamine metabolism-related core prognostic biomarkers in GBMLGG

TCGA-GBMLGG analysis identified 20 PMRGs (e.g., ODC1, PSMB9) upregulated in disease versus controls **(Figure 1A)**. Univariate Cox analysis showed 13 genes (e.g., PSMA3, PSMB4) linked to poor survival **(Figure 1B, Table S5)**. Training and validation confirmed 10 core biomarkers, including PSMB9 (HR = 4.35/2.04) **(Table S6)**.

3.2 Significant differences in related gene expression among different glioma cell lines

Compared to SVG P12 controls, U87 cells showed significantly increased PSMA3 and PSME1; T98G cells showed increased ODC1, PSMB9, PSMA3, PSME2, PSME3 and PSMF1; U251 cells showed increased ODC1, PSMB9, PSMA3, PSME1, PSME2 and PSME3 **(Figure 1C)**.

3.3 PSMB9 promoted proliferation, migration, invasion and colony formation of T98G glioma cells

WB and RT-qPCR confirmed successful PSMB9 overexpression (OE-PSMB9) and knockdown

(shPSMB9-1/2/3) models in T98G cells, with protein and mRNA levels significantly increased or decreased versus controls (P <0.01 or P <0.001) **(Figure 1D, E)**. Functionally, transwell invasion assay showed OE-PSMB9 increased invading cells while shPSMB9 decreased them versus controls (P <0.01) **(Figure 1F)**. Wound healing assay at 48h demonstrated longer migration distance in OE-PSMB9 and shorter in shPSMB9 versus controls (P <0.001) **(Figure 1G)**. CCK-8 assay revealed greater OD_{450} increase in OE-PSMB9 (P <0.001) and smaller increase in shPSMB9 (48h: P <0.01, 72h: P <0.001) **(Figure 1H)**. Colony formation assay showed higher rate in OE-PSMB9 (P <0.001) and lower rate in shPSMB9 (P <0.01) versus controls **(Figure 1I)**. Collectively, PSMB9 promotes T98G glioma cell proliferation, migration, invasion and colony formation.

3.4 Elevated PSMB9 levels were significantly associated with adverse prognosis in GBMLGG

PSMB9 was markedly upregulated in GBMLGG versus controls (P <0.01) **(Figure 2A)**. In both training and validation sets, high PSMB9 expression correlated with significantly reduced survival versus low expression (P <0.0001) **(Figure 2B)**.

3.5 Association of PSMB9 expression with clinical characteristics and molecular mechanisms in GBMLGG

PSMB9 expression was significantly elevated in patients >65 years, IDH wild-type, and high-grade tumors, and strongly associated with IDH status and MGMT methylation (P <0.001) **(Figure 2C, D)**. GSEA showed PSMB9-related genes enriched in immune-associated KEGG pathways like allograft rejection **(Figure 2E)**. GSVA indicated high-expression group enriched in immune pathways like proteasome, while low-expression group in taste transduction (all P<0.001) **(Figure 2F)**. Differential analysis identified 1346 DEGs (894 upregulated, 452 downregulated) **(Figure 2G)**. GO enrichment involved leukocyte-mediated immunity (BP), collagen-containing extracellular matrix (CC), enzyme

inhibitor activity (MF) **(Figure 2H)**; KEGG enrichment involved phagosome and HTLV-1 infection pathways **(Figure 2I)**. Collectively, PSMB9 emerges as a functionally relevant mediator of GBMLGG progression through immune pathway perturbation, while indicating poor prognostic subsets.

3.6 Association of PSMB9 with immune microenvironment and immune escape in GBMLGG

Analysis of PSMB9-immune microenvironment interactions in GBMLGG revealed that high PSMB9 expression was associated with significantly higher proportions of M2 macrophages and regulatory T cells, and lower monocyte proportion (all P <0.01) **(Figure 3A, B)**, higher TIDE score (r = 0.2, P <1.8 × 10^{-7}) and higher ImmuneScore, StromalScore and Estimate score (all P <0.0001) **(Figure 3C, D)**. PSMB9 expression in C4 subtype exceeded the levels observed in C1, C5, and all other immune subtypes (P <0.05) **(Figure 3E)**.

3.7 Association of PSMB9 expression with gene mutation and drug sensitivity in GBMLGG

Somatic mutation analysis revealed significantly higher TTN (30% vs. 13%) and EGFR (18% vs. 4%) mutation rates in the PSMB9-high group, whereas IDH1 mutations were more frequent in the PSMB9-low group (80% vs. 30%) **(Figure 3F)**. 157 drugs showed significant inter-group differences in IC_{50}, the high-expression group had a significantly lower IC_{50} for Camptothecin, Irinotecan, Temozolomide and a significantly higher IC_{50} for Carmustine **(Figure 3G)**. These findings nominate PSMB9 as a molecular hub connecting oncogenic mutation patterns to therapeutic vulnerabilities in glioma.

3.8 Analysis of DEGs and molecular networks after PSMB9 knockdown

PSMB9 expression in the T98G-SH-PSMB9 demonstrated significantly attenuated expression relative to T98G **(Figure 4A)**, a total of 1924 PSMB9-DEGs were identified (998 upregulated, 926 downregulated), with volcano and heat maps showing their distribution and expression patterns

(Figure 4B). 89 interacting proteins such as TAP1 and UBA7 were obtained via STRING PPI network **(Figure 4C)**, 15 genes such as CDC20 and HLA-F strongly correlated with PSMB9 were screened out ($|r| > 0.9$, $P < 0.05$), the correlation heatmap provided an intuitive visualization of the strong association characteristics of these genes with PSMB9 **(Figure 4D)**. These findings provide core candidate genes for subsequent validation and mechanism exploration of PSMB9.

3.9 Expression and prognostic analysis of PSMB9-related key genes

The analysis of the association between PSMB9 and key gene showed that CDC20, HLA-F, TAP1 and UBA7 were significantly overexpressed in TCGA-GBMLGG group vs control, and downregulated in the T98G-SH-PSMB9 **(Figure 4E)**. KM curves indicated that high expression of these 4 genes was associated with significantly lower survival rate ($P < 0.0001$), serving as survival risk factors **(Figure 4F)**. These findings confirm key genes associated with PSMB9, whose high expression correlates with poor prognosis.

3.10 HLA-F mediated PSMB9-driven glioma malignancy

Compared with controls, T98G showed slight CDC20 decrease and significant HLA-F increase, with no notable changes in TAP1 or UBA7. T98G-SH-PSMB9 showed significant downregulation of all four genes, indicating PSMB9 positively regulates their expression **(Figure 5A)**. HLA-F knockdown (sh-HLA-F-1/2/3) significantly reduced protein and mRNA levels, while overexpression (OE-HLA-F) markedly increased them ($P < 0.001$), confirming successful cell line establishment **(Figure 5B)**. Functional assays showed OE-HLA-F enhanced viability, migration, invasion and colony formation, whereas sh-HLA-F suppressed them, demonstrating HLA-F promotes glioma malignancy **(Figure 5C-F)**. Finally, in PSMB9-knockdown background, further HLA-F silencing exacerbated inhibition of malignant phenotypes, while HLA-F overexpression reversed these effects **(Figure 5G-J)**, confirming

HLA-F as a key downstream effector of PSMB9, and the two synergistically drive glioma malignant progression.

3.11 *In vivo* tumorigenicity of T98G was reduced by target gene knockdown

To investigate PSMB9's oncogenic role *in vivo*, PSMB9 depletion significantly impaired glioma growth, with reduced tumor volumes in T98G-KO versus T98G on days 20 and 25 (P <0.05) **(Figure 6A, Table S7)**. Tumor weight in T98G-KO was also significantly reduced (0.33g vs 0.71g, P = 0.039) **(Figure 6B, Table S8)**. These findings demonstrate PSMB9 knockdown inhibits *in vivo* tumorigenic capacity, indicating PSMB9 exerts a pro-tumorigenic effect on glioma growth in vivo.

3.12 Effect of combined expression of PSMB9 and key genes on prognosis of GBMLGG patients

High-high co-expression groups (PSMB9 + CDC20, PSMB9 + TAP1, PSMB9 + UBA7) exhibited significantly reduced survival versus other subgroups, low-low combinations showed highest survival rates (all P <0.001). Notably, the PSMB9 + HLA-F pair showed weaker survival differences **(Figure S1A-D)**. These suggest that the combination of high expression of PSMB9 and key genes can enhance the predictive ability for poor prognosis.

4 Discussion

This study identified 10 PMRGs differentially expressed in gliomas via bioinformatics. Among them, PSMB9 was highly expressed in T98G and U251 cells. Overexpression promoted proliferation, migration, invasion and colony formation, while knockdown inhibited these malignant phenotypes. High PSMB9 expression correlated with abnormal immune infiltration, immune evasion, distinct mutation profiles and enhanced camptothecin sensitivity. HLA-F was identified as a key downstream target, with functional validation confirming PSMB9 positively regulates HLA-F, and the PSMB9-HLA-F axis jointly drives glioma malignant progression.

Proteasome subunit beta type-9 (PSMB9) is a member of the proteasome beta subunit family and encodes the pivotal β1i component of the immunoproteasome [28]. There is considerable evidence indicating that PSMB9 serves as a prognostic factor for various autoimmune diseases [29-31]. Recent studies highlighted that PSMB9 expression is significantly deregulated in tumors, and PMSB9 orchestrates key immune processes within the tumor microenvironment and serves as a potent biomarker for patient prognosis [32]. In hepatocellular carcinoma (HCC), in vitro assays confirmed that PSMB9 overexpression enhanced proliferation, migration, and resistance to apoptosis in HepG2 cells [33]. The present research outcomes showed that PSMB9 is significantly overexpressed in T98G, U251 cell lines, and is closely associated with high tumor grade, IDH wild-type phenotype, and short survival time in patients, making it an independent prognostic marker for glioma. This is consistent with research findings in hepatocellular carcinoma, where high expression of PSMB9 was found to promote tumor invasion and correlate with poor prognosis, suggesting that the function of PSMB9 as an oncogene may be conserved across different tumors.

The present study reveals a novel association between PSMB9 and polyamine metabolism in glioma. Previous studies have shown that the function of PSMB9 mainly focuses on the core components of immune proteasome [34], and regulating macrophage infiltration [35]. In tumors, the influence of PSMB9 has been found to include regulating tumor immune microenvironment [36], participating in antigen processing and presentation [37], and affecting the efficacy of immunotherapy [38]. In our study, bioinformatics analysis revealed a significant correlation between PSMB9 and multiple genes related to polyamine metabolism. PSMB9 is not a classical direct association pathway with polyamine metabolism, but there are potential indirect regulation mechanisms. The key enzymes involved in polyamine metabolism can be degraded by the proteasome [39], while PSMB9 is a key component of

353 the proteasomet [34], may indirectly participate in the regulation of polyamine metabolism by affecting
354 the overall activity or substrate selectivity of the proteasome in the tumor microenvironmen. No direct
355 link between PSMB9 and polyamine metabolism has been reported, and the upstream regulation of
356 polyamine metabolism remains unknown. This study fills that gap by extending PSMB9's role from
357 immunity to metabolic regulation. Future work will explore whether PSMB9 regulates polyamine
358 metabolism via proteasomal activity or non-canonical functions.
359 This study clarified the upstream and downstream regulatory relationship between PSMB9 and Human
360 leukocyte antigen F(HLA-F). Through bioinformatics analysis, HLA-F was identified as a candidate
361 downstream target gene of PSMB9. Subsequently, we discovered that knocking down PSMB9 can
362 downregulate the mRNA and protein levels of HLA-F *in vitro*. Overexpressing HLA-F while knocking
363 down PSMB9 can partially reverse the inhibition of cell proliferation, migration, invasion, and
364 colony-forming ability caused by PSMB9 knockdown. HLA-F is a non-classical MHC class I molecule
365 (MHC-Ib) that regulates the immune system during pregnancy, infection, and autoimmune processes. It
366 primarily regulates immune response by interacting with receptors on the surface of natural killer (NK)
367 cells and $CD8^+$ T cells, and promotes immune tolerance [40]. Tumours similarly exploit HLA-F to
368 evade immune detection and promote tumor progression [41]. Studies have shown that that HLA-F
369 expression was found to be elevated in gliomas, and positively correlated with malignant phenotype
370 and negatively correlated with overall survival [42]. Previous findings identify PSMB9 is tightly linked
371 to immune-related pathways, including IFN-γ responses and antigen presentation, and its expression
372 positively correlates with infiltration of $CD8^+$ T cells, dendritic cells, and macrophages in the tumor
373 microenvironment [32]. This study first identifies PSMB9 as an upstream positive regulator of HLA-F.
374 As both are involved in antigen processing/presentation, their regulation may reflect intrinsic synergy

within the proteasome-antigen presentation pathway. The specific mechanism (e.g., transcription factors or epigenetic modifications) warrants further investigation.

This study found that drug sensitivity analysis based on the GDSC database revealed that the IC50 values for camptothecin and irinotecan were significantly lower in the PSMB9 high-expression group compared to the low-expression group, while the IC50 value for carmustine was significantly higher. High expression of PSMB9 is associated with increased sensitivity to camptothecin-based drugs and resistance to carmustine, suggesting that PSMB9 has potential value as a predictive biomarker for chemotherapy response. camptothecin is a DNA topoisomerase I inhibitor, exerting its anti-tumor effect by blocking DNA reconnection and causing lethal double-strand breaks during DNA replication [43]. Abnormal expression of metabolism-related genes can regulate chemosensitivity, and abnormal activation of polyamines is closely related to chemotherapy resistance. Elevated polyamine levels can reduce the sensitivity of glioma cells to temozolomide by inhibiting apoptosis, promoting DNA damage repair, regulating drug transporter expression, enhancing autophagic flux, or inhibiting the mitochondrial apoptosis pathway [44,45]. Since PSMB9 positively regulates polyamine metabolism and its overexpression confers camptothecin sensitivity, PSMB9 may affect drug response via two mechanisms: regulating polyamine metabolism to alter DNA replication stress/topoisomerase activity, or modulating antigen presentation and immune microenvironment as an immunoproteasome subunit. Conversely, PSMB9 overexpression showed resistance to carmustine, suggesting differential regulation across chemotherapeutics. This study preliminarily links PSMB9, polyamine metabolism and chemosensitivity, offering potential biomarkers for individualized glioma chemotherapy. Future larger cohort validation and mechanistic elucidation are warranted.

This study innovatively identified PSMB9 from polyamine metabolism perspective, established the

PSMB9-HLA-F regulatory axis via a bioinformatics-to-in-vivo verification strategy, filling a cross-field research gap. Limitations include lack of multi-ethnic validation, undetected polyamine metabolites, unclear PSMB9-HLA-F mechanism, and heterotopic model constraints. Despite these, the PSMB9-HLA-F axis offers new prognostic and therapeutic targets for glioma.

5 Conclusion

The present study showed that PSMB9 regulates polyamine metabolism by up-regulating HLA-F and promotes the malignant progression of glioma. PSMB9 and HLA-F can be used as potential targets for prognosis evaluation and targeted therapy of glioma.

Statements and Declarations

Funding

This work was supported by the special fund for Science and Technology Innovation Teams of Shanxi Province under Grant number 202304051001045.

Competing interests

The authors declares that there is no conflict of interest.

Author contributions

Yan Cheng: Conceptualization, Project administration, Writing-original draft, Writing-review &editing; Lin Zhang and Lina Zheng: Investigation, Methodology, Validation; Ting Wang: Investigation, Visualization; Weiwei Zhang: Funding acquisition. All authors reviewed and approved the final version of the manuscript and agree to be accountable for all aspects of the work.

Ethics approval

All animal experiments were approved by the Animal Ethics Committee of Dr.Can Biotechnology

(Zhejiang) Co., Ltd., Approval No. DRK-20251020212.

Consent to participate

Not applicable.

Consent to publish

Not applicable.

Data availability statement

The data used in this study were obtained from the UCSC Xena database (https://xenabrowser.net/datapages/), the Chinese Glioma Genome Atlas database (http://www.cgga.org.cn/), and the Molecular Signatures Database (https://www.gsea-msigdb.org/gsea/msigdb). Other data generated during this study are available from the corresponding author upon reasonable request.

Acknowledgments

We would like to express our sincere gratitude to all individuals and organizations who supported and assisted us throughout this research.

Reference

1. Weller M, Wen PY, Chang SM, Dirven L, Lim M, Monje M, Reifenberger G (2024) Glioma. Nature reviews Disease primers 10 (1):33. doi:10.1038/s41572-024-00516-y

2. van den Bent MJ, Geurts M, French PJ, Smits M, Capper D, Bromberg JEC, Chang SM (2023) Primary brain tumours in adults. Lancet (London, England) 402 (10412):1564-1579. doi:10.1016/s0140-6736(23)01054-1

3. Woodworth GF, Anastasiadis P, Ozair A, Chabros J, Bettegowda C, Chen C, Gerstl JVE, Douville C, Mekary RA, Smith TR, Meng Y, Hawkins C, Pople CB, Abrahao A, Llinas M, Heyn C, Bunevicius A, Rezai AR, Ball AJS, Henry K, Sahgal A, Torio E, Ren H, Ahmad H, Arora H, Eisenberg H, Perry J, Carpenter JS, Hynynen K, Pham LC, Anketell MB, Lim-Fat MJ, Xu Z, Cifarelli CP, Sheehan JP, McDannold NJ, Gandhi D, Golby AJ, Lipsman N (2025) Microbubble-enhanced transcranial focused ultrasound with temozolomide for patients with high-grade glioma (BT008NA): a multicentre, open-label, phase 1/2 trial. The Lancet Oncology 26 (12):1651-1664. doi:10.1016/s1470-2045(25)00492-9

4. Wang Y, Pan C, Xie M, Zuo P, Li X, Gu G, Li T, Jiang Z, Wu Z, Zhang J, Zhang L (2022) Adult diffuse intrinsic pontine glioma: clinical, radiological, pathological, molecular features, and treatments of 96 patients. Journal of neurosurgery 137 (6):1628-1638. doi:10.3171/2022.2.Jns211920

5. Schaff LR, Mellinghoff IK (2023) Glioblastoma and Other Primary Brain Malignancies in Adults: A Review. Jama 329 (7):574-587. doi:10.1001/jama.2023.0023

6. Ostrom QT, Price M, Neff C, Cioffi G, Waite KA, Kruchko C, Barnholtz-Sloan JS (2022) CBTRUS Statistical Report: Primary Brain and Other Central Nervous System Tumors Diagnosed in the United States in 2015-2019. Neuro-oncology 24 (Suppl 5):v1-v95. doi:10.1093/neuonc/noac202

7. Xuan M, Gu X, Li J, Huang D, Xue C, He Y (2023) Polyamines: their significance for maintaining health and contributing to diseases. Cell communication and signaling : CCS 21 (1):348. doi:10.1186/s12964-023-01373-0

8. Holbert CE, Cullen MT, Casero RA, Jr., Stewart TM (2022) Polyamines in cancer: integrating organismal metabolism and antitumour immunity. Nature reviews Cancer 22 (8):467-480. doi:10.1038/s41568-022-00473-2

9. Murray-Stewart TR, Woster PM, Casero RA, Jr. (2016) Targeting polyamine metabolism for cancer therapy and prevention. The Biochemical journal 473 (19):2937-2953. doi:10.1042/bcj20160383

10. Arruabarrena-Aristorena A, Zabala-Letona A, Carracedo A (2018) Oil for the cancer engine: The cross-talk between oncogenic signaling and polyamine metabolism. Science advances 4 (1):eaar2606. doi:10.1126/sciadv.aar2606

11. Nakanishi S, Cleveland JL (2021) Polyamine Homeostasis in Development and Disease. Medical sciences (Basel, Switzerland) 9 (2). doi:10.3390/medsci9020028

12. Kim JH, Lee ST (2022) Polyamine Oxidase Expression Is Downregulated by 17β-Estradiol via Estrogen Receptor 2 in Human MCF-7 Breast Cancer Cells. International journal of molecular sciences 23 (14). doi:10.3390/ijms23147521

13. Gamble LD, Purgato S, Murray J, Xiao L, Yu DMT, Hanssen KM, Giorgi FM, Carter DR, Gifford AJ, Valli E, Milazzo G, Kamili A, Mayoh C, Liu B, Eden G, Sarraf S, Allan S, Di Giacomo S, Flemming CL, Russell AJ, Cheung BB, Oberthuer A, London WB, Fischer M, Trahair TN, Fletcher JI, Marshall GM, Ziegler DS, Hogarty MD, Burns MR, Perini G, Norris MD, Haber M (2019) Inhibition of polyamine synthesis and uptake reduces tumor progression and prolongs survival in mouse models of neuroblastoma. Science translational medicine 11 (477). doi:10.1126/scitranslmed.aau1099

14. Ernestus RI, Röhn G, Schröder R, Els T, Klekner A, Paschen W, Klug N (2001) Polyamine metabolism in brain tumours: diagnostic relevance of quantitative biochemistry. Journal of neurology, neurosurgery, and psychiatry 71 (1):88-92. doi:10.1136/jnnp.71.1.88

15. Gustavsson EK, Zhang D, Reynolds RH, Garcia-Ruiz S, Ryten M (2022) ggtranscript: an R package for the visualization and interpretation of transcript isoforms using ggplot2. Bioinformatics (Oxford, England) 38 (15):3844-3846. doi:10.1093/bioinformatics/btac409

16. Rizvi AA, Karaesmen E, Morgan M, Preus L, Wang J, Sovic M, Hahn T, Sucheston-Campbell LE (2019) gwasurvivr: an R package for genome-wide survival analysis. Bioinformatics (Oxford, England) 35 (11):1968-1970. doi:10.1093/bioinformatics/bty920

17. Xiao C, Zhang X, Hou B, Wan P, Cao Z, Rao X (2024) CYFIP2: potential pancreatic cancer biomarker and immunotherapeutic target. Discover oncology 15 (1):847. doi:10.1007/s12672-024-01650-5

18. Yu G, Wang LG, Han Y, He QY (2012) clusterProfiler: an R package for comparing biological themes among gene clusters. Omics : a journal of integrative biology 16 (5):284-287. doi:10.1089/omi.2011.0118

19. Hänzelmann S, Castelo R, Guinney J (2013) GSVA: gene set variation analysis for microarray and RNA-seq data. BMC bioinformatics 14:7. doi:10.1186/1471-2105-14-7

20. Liu S, Wang Z, Zhu R, Wang F, Cheng Y, Liu Y (2021) Three Differential Expression Analysis Methods for RNA Sequencing: limma, EdgeR, DESeq2. Journal of visualized experiments : JoVE (175). doi:10.3791/62528

21. Chen B, Khodadoust MS, Liu CL, Newman AM, Alizadeh AA (2018) Profiling Tumor Infiltrating Immune Cells with CIBERSORT. Methods in molecular biology (Clifton, NJ) 1711:243-259. doi:10.1007/978-1-4939-7493-1_12

22. Yoshihara K, Shahmoradgoli M, Martínez E, Vegesna R, Kim H, Torres-Garcia W, Treviño V, Shen H, Laird PW, Levine DA, Carter SL, Getz G, Stemke-Hale K, Mills GB, Verhaak RG (2013) Inferring tumour purity and stromal and immune cell admixture from expression data. Nature communications 4:2612. doi:10.1038/ncomms3612

23. Wang YW, Ané C (2022) KIMGENS: a novel method to estimate kinship in organisms with mixed haploid diploid genetic systems robust to population structure. Bioinformatics (Oxford, England) 38 (11):3044-3050. doi:10.1093/bioinformatics/btac293

24. Li H, Luo B, Tulufu Y, Wang X, Yue D (2025) A super-enhancer-related gene signature predicts prognosis and immune microenvironment features in glioma. Cellular and molecular biology (Noisy-le-Grand, France) 71 (6):102-109. doi:10.14715/cmb/2025.71.6.14

25. Mayakonda A, Lin DC, Assenov Y, Plass C, Koeffler HP (2018) Maftools: efficient and comprehensive analysis of somatic variants in cancer. Genome research 28 (11):1747-1756. doi:10.1101/gr.239244.118

26. Maeser D, Gruener RF, Huang RS (2021) oncoPredict: an R package for predicting in vivo or cancer patient drug response and biomarkers from cell line screening data. Briefings in bioinformatics 22 (6). doi:10.1093/bib/bbab260

27. Pertea M, Kim D, Pertea GM, Leek JT, Salzberg SL (2016) Transcript-level expression analysis of RNA-seq experiments with HISAT, StringTie and Ballgown. Nature protocols 11 (9):1650-1667. doi:10.1038/nprot.2016.095

28. Leone P, Shin EC, Perosa F, Vacca A, Dammacco F, Racanelli V (2013) MHC class I antigen processing and presenting machinery: organization, function, and defects in tumor cells. Journal of the National Cancer Institute 105 (16):1172-1187. doi:10.1093/jnci/djt184

29. Li S, He RC, Wu SG, Song Y, Zhang KL, Tang ML, Bei YR, Zhang T, Lu JB, Ma X, Jiang M, Qin LJ, Xu Y, Dong XH, Wu J, Dai X, Hu YW (2024) LncRNA PSMB8-AS1 Instigates Vascular Inflammation to Aggravate Atherosclerosis. Circulation research 134 (1):60-80. doi:10.1161/circresaha.122.322360

30. Zeng L, Chen K, Xiao F, Zhu CY, Bai JY, Tan S, Long L, Wang Y, Zhou Q (2023) Potential common molecular mechanisms between Sjögren syndrome and inclusion body myositis: a bioinformatic analysis and in vivo validation. Frontiers in immunology 14:1161476. doi:10.3389/fimmu.2023.1161476

31. Li Z, Chen Y, Zulipikaer M, Xu C, Fu J, Deng T, Hao LB, Chen JY (2022) Identification of PSMB9 and CXCL13 as Immune-related Diagnostic Markers for Rheumatoid Arthritis by Machine Learning. Current pharmaceutical design 28 (34):2842-2854. doi:10.2174/1381612828666220831085608

32. Ma X, Zhu Q, Wu Z, Han W (2025) PSMB9 Orchestrates Tumor Immune Landscape and Serves as a Potent Biomarker for Prognosis and T Cell-Based Immunotherapy Response. Current issues in molecular biology 47 (9). doi:10.3390/cimb47090712

33. Liu Y, Cao J, Yu H, Sun Q, Zhu T, Zhou YU, Ding X, Wang J, Guo X, Wu Z (2026) Dual Role of PSMB9 Linking Immune Activation and Tumor Adaptation in Hepatocellular Carcinoma With Therapeutic and Prognostic Implications. Anticancer research 46 (3):1389-1410. doi:10.21873/anticanres.18036

34. Wang X, Meul T, Meiners S (2020) Exploring the proteasome system: A novel concept of proteasome inhibition and regulation. Pharmacology & therapeutics 211:107526. doi:10.1016/j.pharmthera.2020.107526

35. Zhang C, Lio C, Li N, Yu Y, Luo J (2026) Sinomenine Regulates PSMB9 to Mediate Therapeutic Effects in Rheumatoid Arthritis. Cells 15 (11). doi:10.3390/cells15111005

36. Wang X, You H, Zhang T, Li Y, Chen X, Basler M, Jiang Q, Chen H, Liu N, Yuan F, Li J (2025) Immunoproteasome subunits are novel signatures for predicting efficacy of immunotherapy in muscle invasive bladder cancer. Journal of translational medicine 23 (1):228. doi:10.1186/s12967-025-06207-w

37. Wiśniewski A, Sobczyński M, Pawełczyk K, Porębska I, Jasek M, Wagner M, Niepiekło-Miniewska W, Kowal A, Dubis J, Jędruchniewicz N, Kuśnierczyk P (2021) Polymorphisms of Antigen-Presenting Machinery Genes in Non-Small Cell Lung Cancer: Different Impact on Disease Risk and Clinical Parameters in Smokers and Never-Smokers. Frontiers in immunology 12:664474. doi:10.3389/fimmu.2021.664474

38. Pan Q, Cheng Y, Cheng D (2021) Identification of CD8+ T Cell-Related Genes: Correlations with Immune Phenotypes and Outcomes of Liver Cancer. Journal of immunology research 2021:9960905. doi:10.1155/2021/9960905

39. Murakami Y, Matsufuji S, Kameji T, Hayashi S, Igarashi K, Tamura T, Tanaka K, Ichihara A (1992) Ornithine decarboxylase is degraded by the 26S proteasome without ubiquitination. Nature 360 (6404):597-599. doi:10.1038/360597a0

40. Dulberger CL, McMurtrey CP, Hölzemer A, Neu KE, Liu V, Steinbach AM, Garcia-Beltran WF, Sulak M, Jabri B, Lynch VJ, Altfeld M, Hildebrand WH, Adams EJ (2017) Human Leukocyte

Antigen F Presents Peptides and Regulates Immunity through Interactions with NK Cell Receptors. Immunity 46 (6):1018-1029.e1017. doi:10.1016/j.immuni.2017.06.002

41. Duhamel M, Cardon T, Ziane-Chaouche L, Salzet M (2026) Nonclassical HLA and pseudogenes in maternal-fetal tolerance and cancer. Trends in immunology 47 (3):220-228. doi:10.1016/j.it.2025.08.006

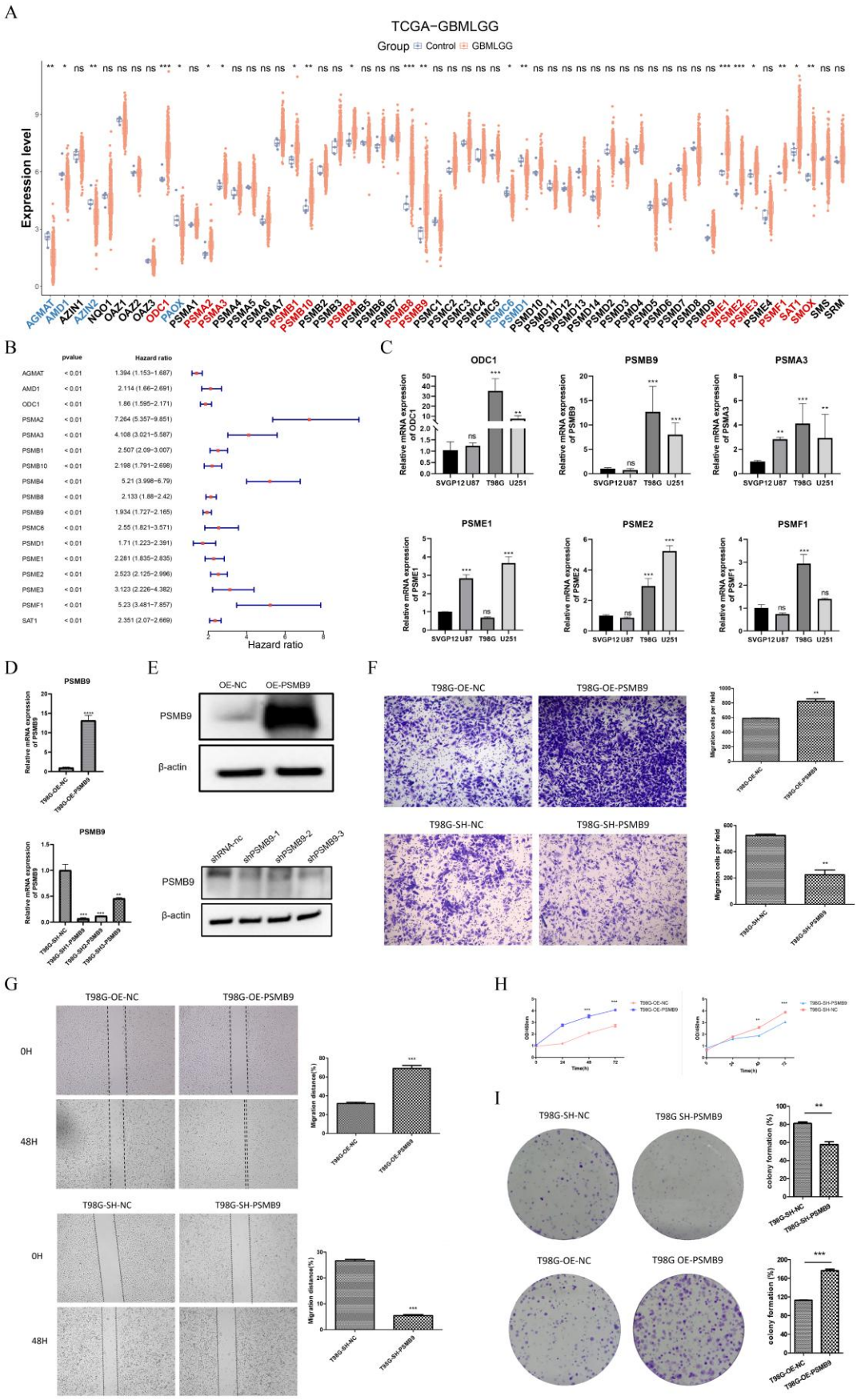
42. Feng E, Liang T, Wang X, Du J, Tang K, Wang X, Wang F, You G (2019) Correlation of alteration of HLA-F expression and clinical characterization in 593 brain glioma samples. Journal of neuroinflammation 16 (1):33. doi:10.1186/s12974-019-1418-3

43. Staker BL, Hjerrild K, Feese MD, Behnke CA, Burgin AB, Jr., Stewart L (2002) The mechanism of topoisomerase I poisoning by a camptothecin analog. Proceedings of the National Academy of Sciences of the United States of America 99 (24):15387-15392. doi:10.1073/pnas.242259599

44. Wei XC, Zhang HQ, Liu GQ, Liu CW, Li AL, Pan X, Yan WQ, Chen JY (2025) ODC-Driven Polyamines Synthesis Sustains the Self-Renewal of Glioblastoma Stem Cells and Drives Tumor Aggressiveness. Cancer science 116 (11):3079-3089. doi:10.1111/cas.70182

45. Chenna SS, Gajula SNR, Nalla LV (2025) Polyamine metabolism in cancer: drivers of immune evasion, ferroptosis and therapy resistance. Expert reviews in molecular medicine 27:e39. doi:10.1017/erm.2025.10026

Figures



585

586 **Figure 1 Screening of core polyamine metabolism-related genes (PMRGs) and PSMB9's effect on**

T98G malignant phenotypes. (A) Differentially expressed PMRGs (DE-PMRGs) in glioblastoma multiforme and lower grade glioma (GBMLGG). **(B)** Univariate Cox analysis of differentially expressed genes (DEGs). **(C)** Related gene expression in different glioma cell lines. **(D)** Reverse Transcription Quantitative Polymerase Chain Reaction (RT-qPCR) validation of PSMB9 stable cell models. **(E)** Western blot (WB) validation of PSMB9 stable cell models. **(F)** Cell invasion by transwell assay. **(G)** Cell migration by scratch assay. **(H)** Cell proliferation by Cell Counting Kit-8 (CCK-8) assay. **(I)** Colony formation ability by colony formation assay. (In the figure, ns denotes no statistically significant difference, * corresponds to $P < 0.05$, ** corresponds to $P < 0.01$, *** corresponds to $P < 0.001$ and **** corresponds to $P < 0.0001$.)

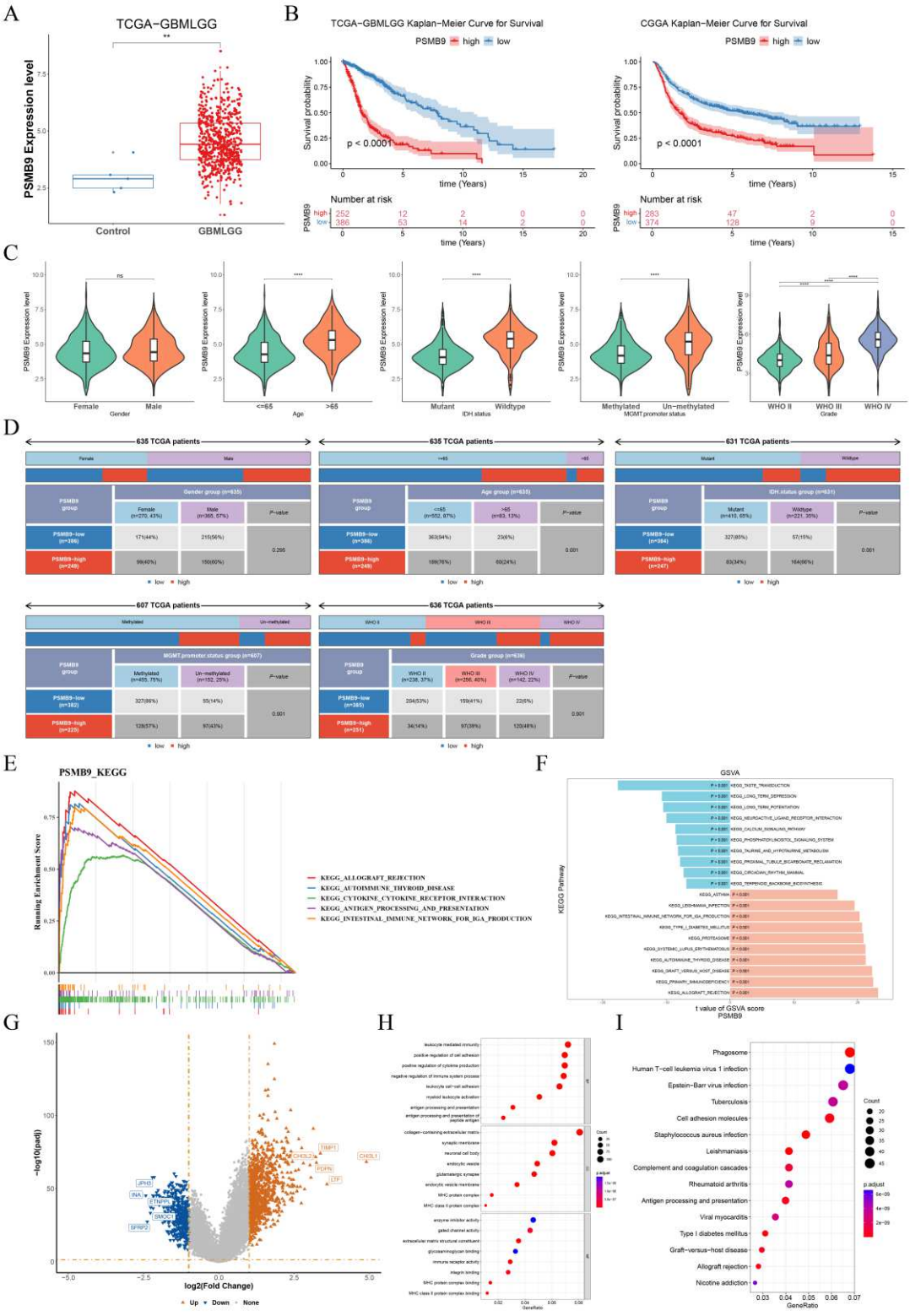


Figure 2 PSMB9 expression, prognostic value and molecular mechanism in GBMLGG. (A) PSMB9 expression in GBMLGG vs control. **(B)** Survival analysis of PSMB9 high/low expression groups (training/validation set). **(C)** PSMB9 expression in different clinical subgroups. **(D)** Correlation

of PSMB9 with clinical features. **(E)** Gene Set Enrichment Analysis (GSEA) enrichment of PSMB9-related genes. **(F)** Gene Set Variation Analysis (GSVA) enrichment of PSMB9 high/low expression groups. **(G)** Volcano plot of PSMB9-related DEGs. **(H)** Gene Ontology (GO) enrichment of DEGs. **(I)** Kyoto Encyclopedia of Genes and Genomes (KEGG) enrichment of DEGs. (In the figure, ns denotes no statistically significant difference, ** corresponds to $P < 0.01$ and **** corresponds to $P < 0.0001$.)

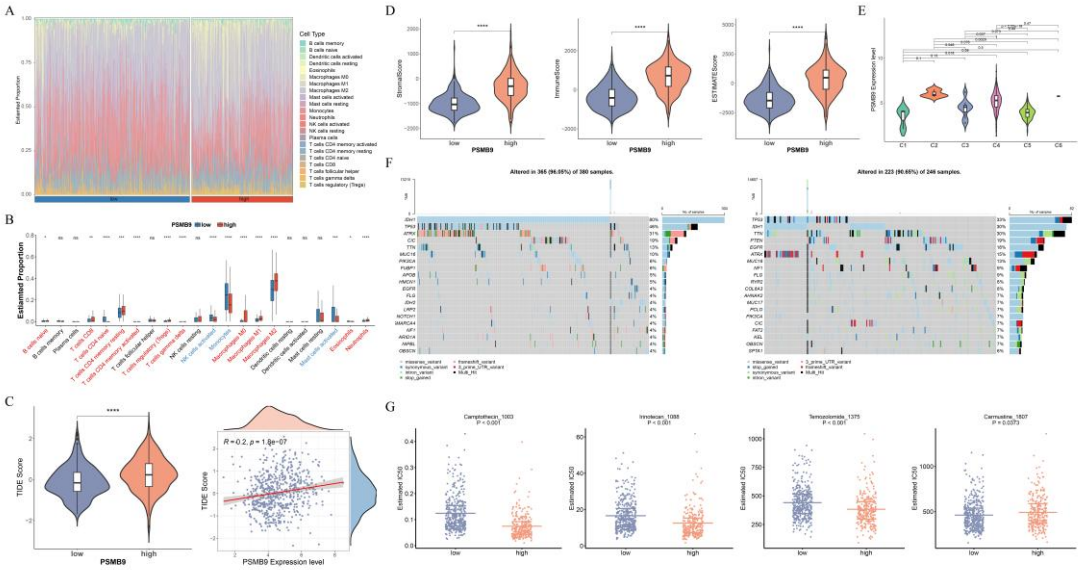


Figure 3 PSMB9 association with immune microenvironment, mutation and drug sensitivity in GBMLGG. (A) Immune cell infiltration in PSMB9 high/low groups. **(B)** Intergroup difference of key immune cell infiltration. **(C)** Correlation and intergroup difference of PSMB9 and Tumor Immune Dysfunction and Exclusion (TIDE) score. **(D)** Immune/Stromal/Estimate score in PSMB9 high/low groups. **(E)** PSMB9 expression in different immune subtypes. **(F)** Mutation waterfall plot of PSMB9 high/low groups. **(G)** Drugs half-maximal inhibitory concentration (IC50) difference in PSMB9 high/low groups. (In the figure, ns denotes no statistically significant difference, * corresponds to $P < 0.05$, ** corresponds to $P < 0.01$, *** corresponds to $P < 0.001$ and **** corresponds to $P < 0.0001$.)

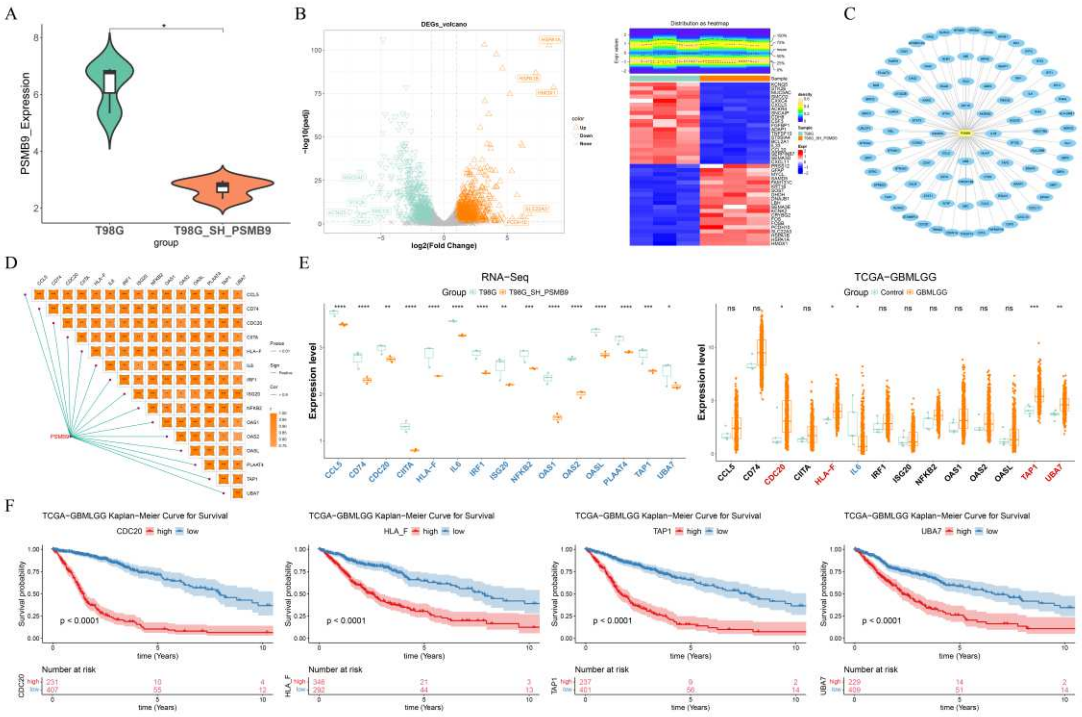


Figure 4 DEG analysis after PSMB9 knockdown and key genes' expression & prognosis. (A) PSMB9 expression validation in PSMB9-knockdown cells. **(B)** Volcano plot and heatmap of DEGs after PSMB9 knockdown. **(C)** Protein-Protein Interaction (PPI) network of PSMB9 and DEGs. **(D)** Correlation heatmap of PSMB9 and interacting genes. **(E)** Key gene expression in GBMLGG and knockdown cells. **(F)** Survival analysis of key gene high/low expression groups. (In the figure, ns denotes no statistically significant difference, * corresponds to $P < 0.05$, ** corresponds to $P < 0.01$, *** corresponds to $P < 0.001$ and **** corresponds to $P < 0.0001$.)

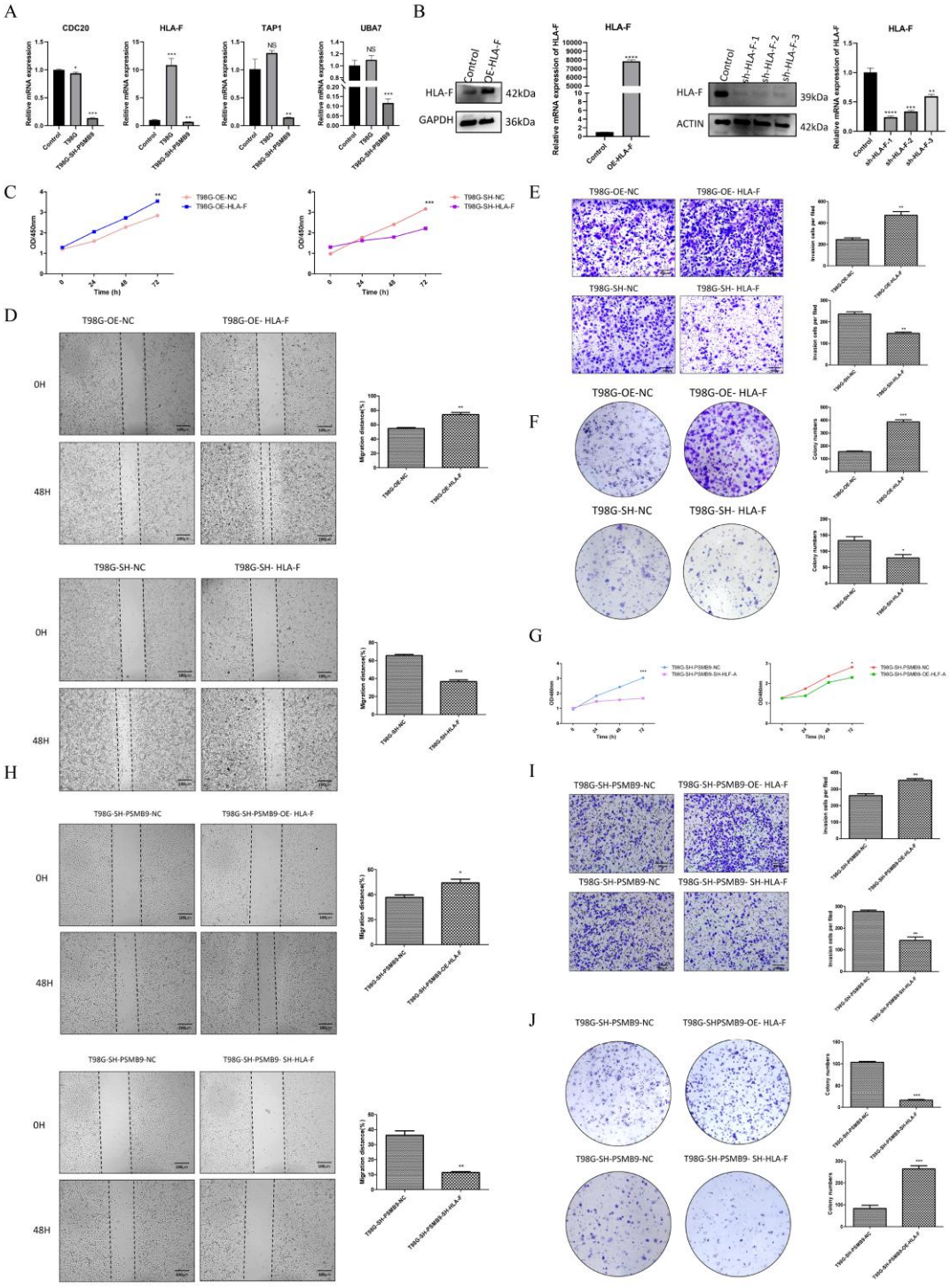


Figure 5 Validation of HLA-F mediating PSMB9-driven glioma malignancy. (A) Effect of PSMB9 knockdown on key gene expression. **(B)** Validation of HLA-F stable cell models (WB/RT-qPCR). **(C)** Effect of HLA-F on cell proliferation. **(D)** Effect of HLA-F on cell migration. **(E)** Effect of HLA-F on cell invasion. **(F)** Effect of HLA-F on colony formation ability. **(G)** Cell proliferation by CCK-8 assay.

(H) Cell migration by scratch assay. **(I)** Cell invasion by transwell assay. **(J)** Colony formation ability by colony formation assay. (In the figure, ns denotes no statistically significant difference, * corresponds to $P < 0.05$, ** corresponds to $P < 0.01$, *** corresponds to $P < 0.001$ and **** corresponds to $P < 0.0001$.)

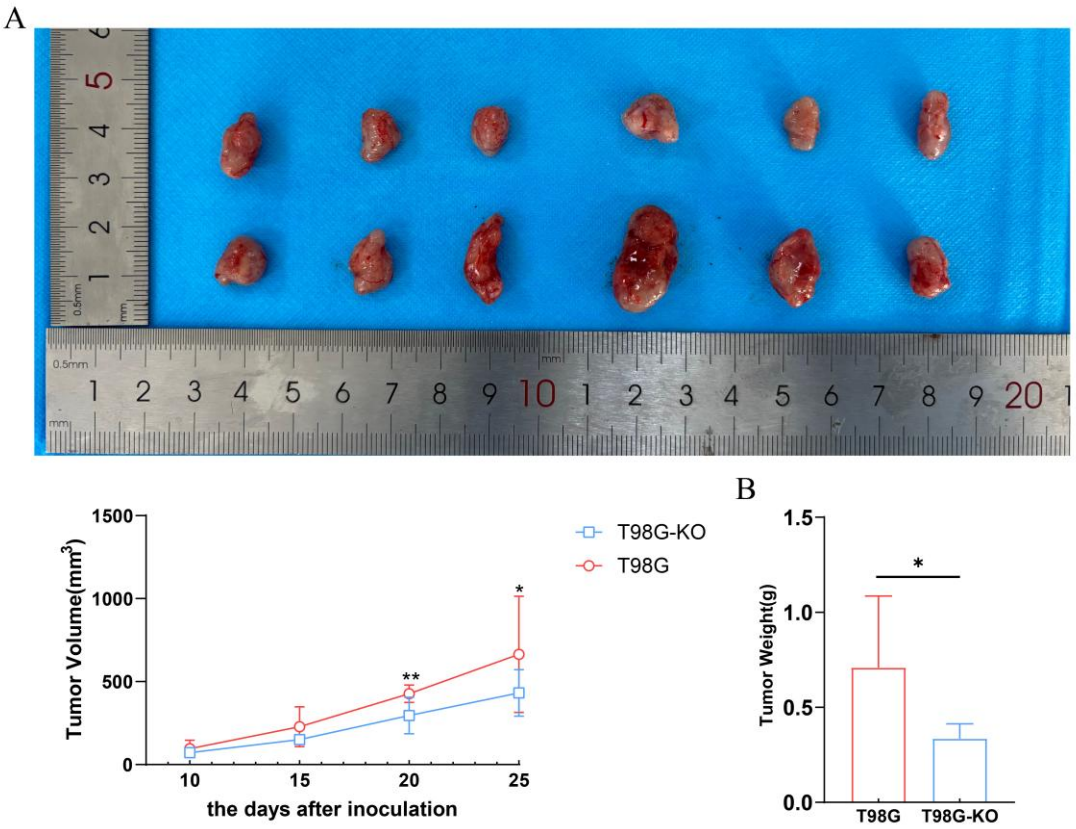


Figure 6 PSMB9 knockdown inhibited T98G tumorigenesis *in vivo*. **(A)** Tumor volume growth curve in nude mice. **(B)** Tumor weight statistics in nude mice.

Supplementary Files

This is a list of supplementary files associated with this preprint. Click to download.

- Westenblotrawimage.docx
- SupplementaryFigure.docx
- SupplementaryTables.docx